Chapter 4

REALIZATION OF PERIODIC AND UNIFORM STRUCTURES FOR COLOUR SEPARATING BACKLIGHTS

Introduction

The rapid developments in information and communication technology in recent years have been facilitated by technological and industrial progress in producing Liquid Crystal Displays (LCDs). For instance, transflective LCDs are widely used in mobile phones or Personal Digital Assistants (PDAs) and transmissive LCDs are commonly employed in notebook computer screens and in desktop computer screens, TV, etc. Both LCD types require an illumination system, a backlight, where light comes to the LCD from behind the screen. Also frontlight systems for reflective LCDs were developed in which the screen is viewed through the frontlight. These reflective LCDs maximise the use of ambient light and consequently the power consumption is reduced. The light losses within both back- or frontlit LCD systems remain however high, and consequently, the displays are limited in brightness, energy efficiency and battery life which is mainly due to light absorption in the polarisers and colour filters. Current customer expectations require these displays to be low cost, low weight, low volume. These factors explain the impetus behind present research and development.

4.1 Liquid Crystal Displays

Liquid Crystal Displays (LCDs) can be classified as passive displays technologies, which means that they do not emit light but modulate incident ambient light or the light of a suitable light source. Hence, LCDs are in fact a electro-optical “light valve”. The most common LCD is the so-called twisted nematic LCD (TN-LCD), which is shown schematically in figure 1:

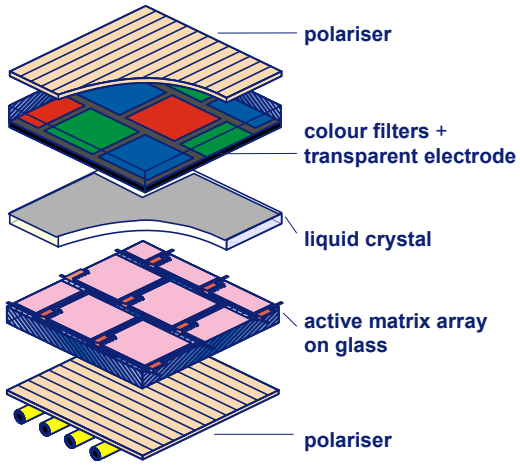

Figure 4.1: Schematic representation of a Twisted Nematic (TN) Liquid Crytal Display cell.

The nematic Liquid Crystal material is situated in the small gap between two glass substrates. The glass plates are covered on the inside with a transparent Indium Tin Oxide (ITO) electrode and with rubbed polyimide orientation layers. The orientation layers impose a uniform orientation of the nematic liquid crystal molecules parallel to the rubbing direction. As the orientation layers at the bottom and top glass slide are crossed, the nematic liquid crystal twists over 90°across the cell. At the outside of the top and bottom glass plates two conventional absorbing polarisers are used parallel to the orientation layers and hence are crossed with respect to each other.

When no voltage is applied to the cell, the incident light is linearly polarized by the first polariser, twisted by the cell over 90° and transmitted through the second polariser (analyser). This is the bright state of the LCD cell. When a sufficient voltage is applied to the cell, the LC molecules will align themselves in the direction of the electric field. Therefore, the twist disappears and the incident light is blocked by the second polariser, resulting in a dark state. Using an intermediate voltage, intermediate brightness levels (grey scales) can be achieved. Furthermore, by adding a red, green or blue (RGB) absorptive color filter to each pixel, also color screens can be produced. By selectively addressing the electric fields of the pixel cells of the display a complete image is produced.

4.2 Colour-separating backlight: principles

Unfortunately, the light management in present liquid crystal displays (LCDs) is not very efficient. We can show in the following schematic representation the typical optical losses of a conventional LCD system:

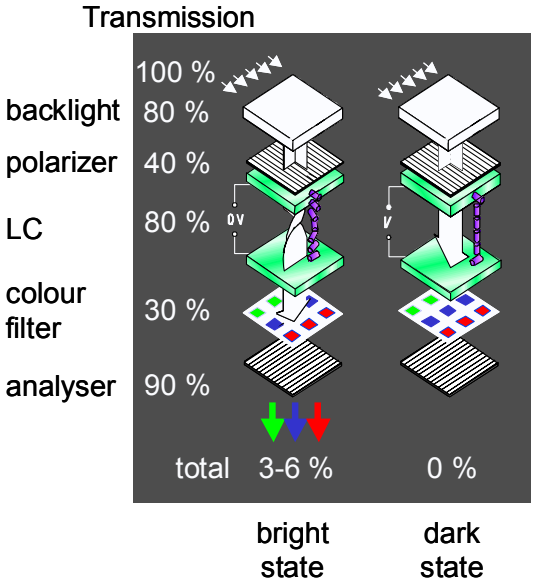

Figure 4.2: Schematic representation of a LCD optical efficiency

Due to at the not perfect connection between backlight and light guide a 20% of loss is present. In order to polarize the source light a standard polariser is used which absorbs another 40% of the incidence radiation. The not perfect alignment of the L.C reduce the remaining radiation, which is ulteriorly attenuated by the colour filter and a second polariser. Finally, the typical efficiency of actual display are about 3-6%.

One of the factors limiting the light throughput is the absorption in the colour filters. It has been shown[34] that a promising way to reduce this absorption is the use of diffractive colour separation by a grating on top of a lightguide in the backlight. Another factor that limits the light throughput is absorption in the polarisers. This absorption can be avoided in a polarised backlight, that is, a backlight that only couples out light of a specific polarisation, e.g. by the use of a birefringent material applied on a microstructured light guide[35,36]. Recently it has been shown[37] that it is possible to combine colour separation with polarised light emission by using of a surface-relief grating with a birefringent coating (Fig 4.3). In that way also the absorption in the polarisers can be reduced.

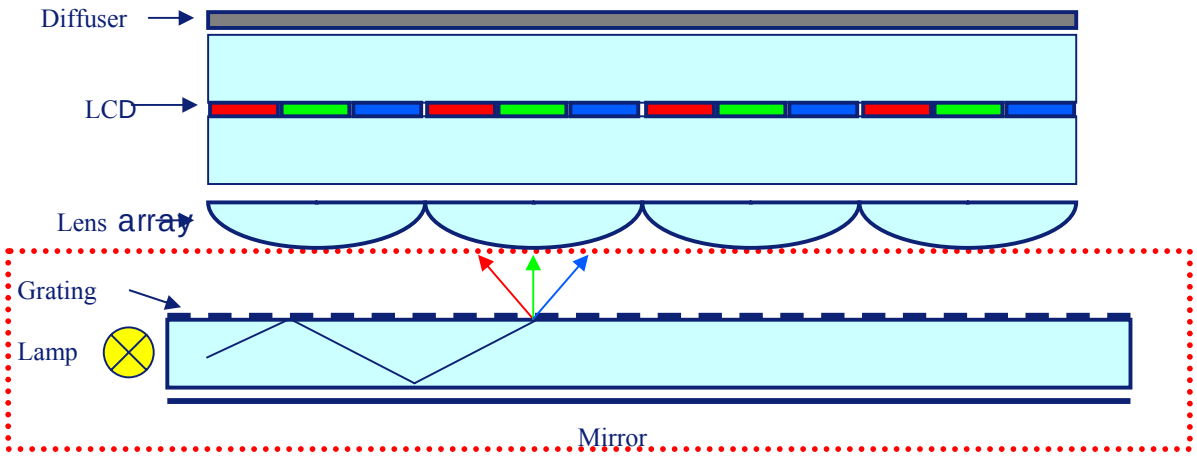

Figure 4.3: LCD system realized with a periodic structures on a light guide.

In this work, the attention has been focalised on the dashed part, namely, the realization of the uniform grating on the light guide in order to obtain a diffractive colour separating. The principle of the colour-separating backlight is as follows (Fig. 4.4).

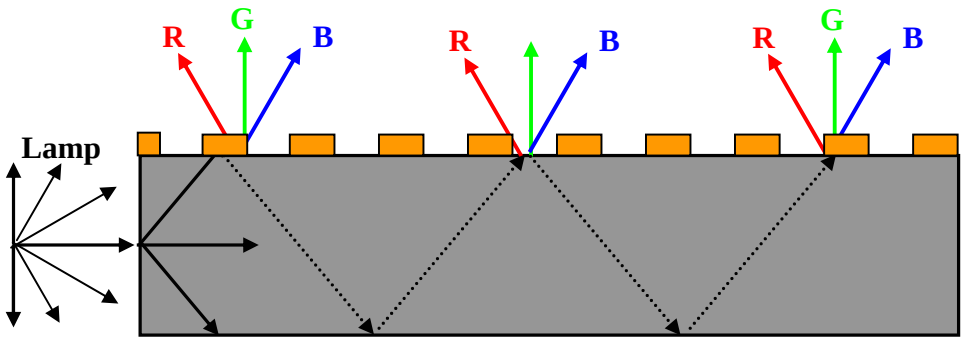

Figure 4.4: Principle of colour-separating backlight consisting of lightguide with grating structure

A surface-relief grating is applied onto a PMMA (poly-methyl methacrylate) lightguide, which is used in a side-lit geometry. Without the grating, the light (we assumed that the lamp emits light in a Lambertian (cosine) way) would be captured inside the lightguide by total internal reflection. The grating causes part of the light to be diffracted into directions both inside and outside the lightguide. If white light is used, red, green and blue light are coupled out in different angular regions. In the case of the colour-separating polarised backlight (Fig. 4.5), the grooves of the grating are filled with a birefringent material having its optical axis along the grooves. The ordinary refractive index (n_o) of the birefringent material is matched to the grating material, whereas its extraordinary refractive index (n_e) is significantly higher.

As a result, light with polarisation along the grooves (s-polarised light) can be diffracted, whereas light with polarisation perpendicular to the grooves (p-polarised light) will propagate unaffectedly in the lightguide due to total internal reflection.

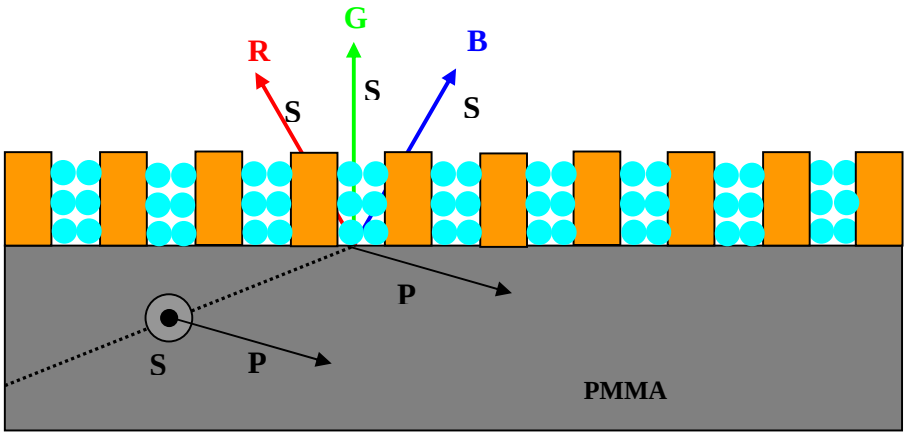

Figure 4.5: Lightguide with grating structure filled with birefringent (LC) layer

Now the outcoupled light has both a high degree of polarisation as well as an angular colour separation.

4.3 Optical Holographic Setup

The experimental setup used in order to realize our gratings is presented in Figure 4.6.

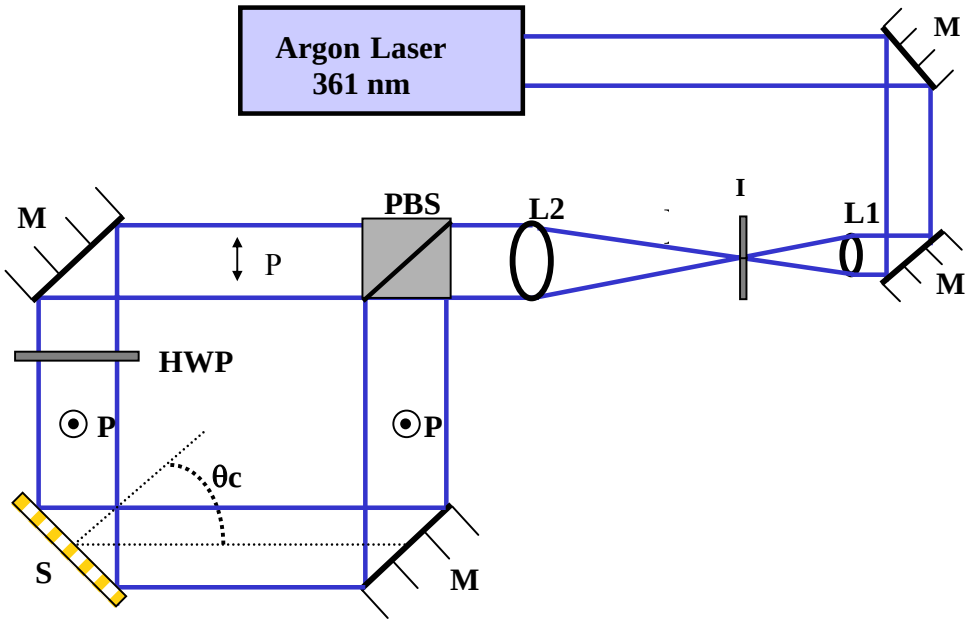

Figure 4.6: Optical setup for UV curing gratings; **M,** mirrors; **L1**, **L2**, lens; **I,** aperture; **PBS,** polariser beam splitter; **HWP**, half-wave plate; **θc**, curing angle; **S**, sample

A single mode beam from an Ar-Ion laser operating at wavelength at 361 nm is broadened by a spatial filter (composed by two lens L1, L2, and a small aperture I) up to a diameter of about 30 mm. It is divided into two beams of nearly the same intensity by the polarising beam splitter PBS. In order to have the same polarization of these two beams, a half-wave plate HWP has been adopted in one of the two arms of the interferometer system. These two beams intersect at the entrance plane of the sample S, giving rise to an interference pattern made of high and low intensity areas whose spatial period depends, as already said, on the interference angle (7, cap 1). The period can be easily varied in the range $\Lambda = 0.2 \approx 15\ \mu m$.

4.4 STABILITY CHECKS

Within the possible sources of noise the stability of the laser source must be considered. The power stability of the laser beam does not affect the fringe visibility *m* of the hologram, because it introduces a variation in both beams simultaneously and hence *m* remains constant. However, a stable output power is required to obtain reproducible exposure conditions. For measuring the power stability of the *Innova Sabre Coherent* UV laser, in our process the following setup was arranged on the optical table:

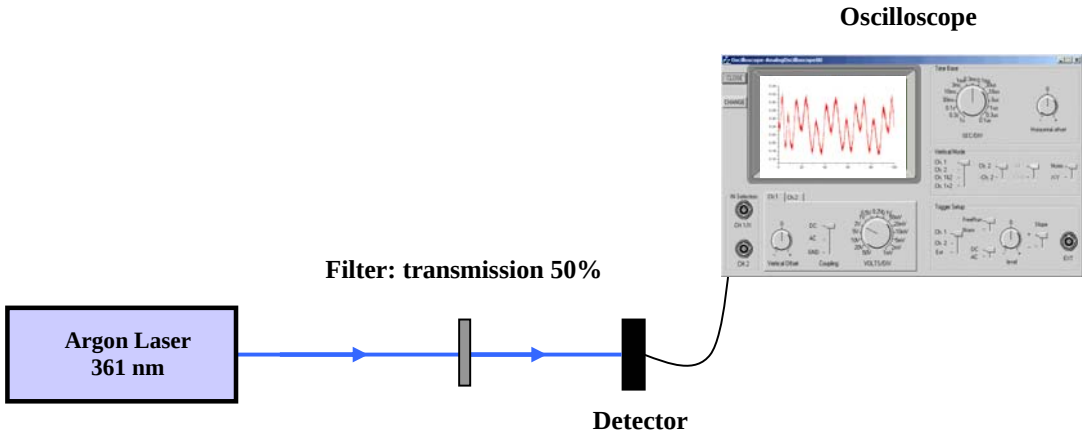

Figure 4.7: Optical setup for measuring of laser power stability

The laser beam is attenuated by a transmission filter in order to avoid the saturation of the used detector. After that, the signal is acquired by a standard oscilloscope. In this way we measure the upper and lower power limits of the laser output and in which way this output varies over time.

Typical results are shown in the following graph:

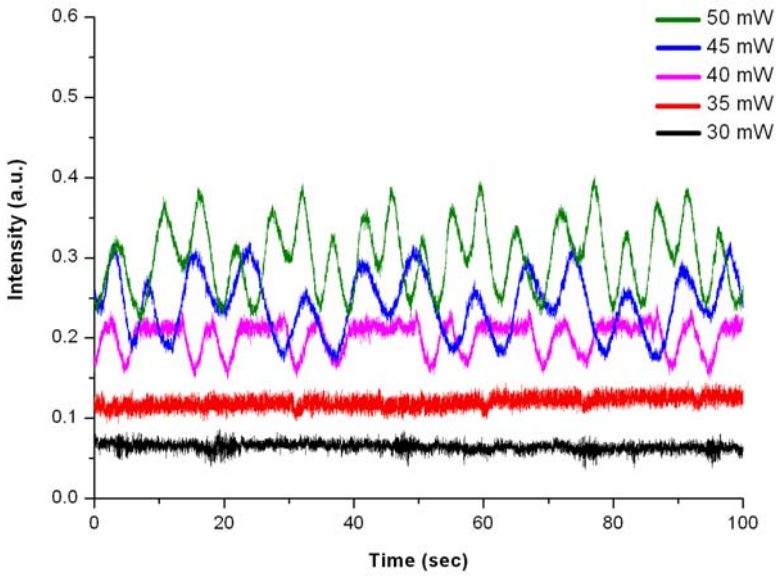

Figure 4.8: Laser beam stability over the time for different power value.

As shown in the figure above, for a low value (30-35 mW) the laser power is almost constant. When the power is increased over 35 mW, the fluctuations become more and more evident and the relative amplitude increases following the power value. Probably this is due to some internal problem related with the power supply or lamps of the laser. We have decided to work in the power range (30-35 mW) in which the laser showed enough stability. Another important source of noise is the wavelength fluctuation of the laser source.

We can show in figure 4.9 what happens to a typical curing geometry in presence of wavelength fluctuations:

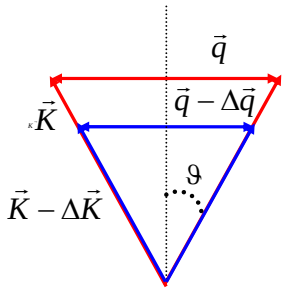

Figure 4.9: Wave vector variation due to the wavelength fluctuation.

As we can see, the red geometry represented the correct condition. Instead the blue geometry takes place if a wavelength fluctuation is present because the wave vector is related to the wavelength by $\vec{k}=\frac{2\pi}{\lambda}$. It is simple to notice that: if a wavelength variation is present (Δλ) this produces a wave vector variation (ΔK). The wave vector of the grating ($\vec{q}$) is related to the wave vector ($\vec{K}$) by equation (7, cap1). This means that a wavelength variation will produce a variation of the wave vector of the grating. In order to check this behavior, we used a Fabry-Perot interferometer system at normal incidence as shown in fig. 4.10:

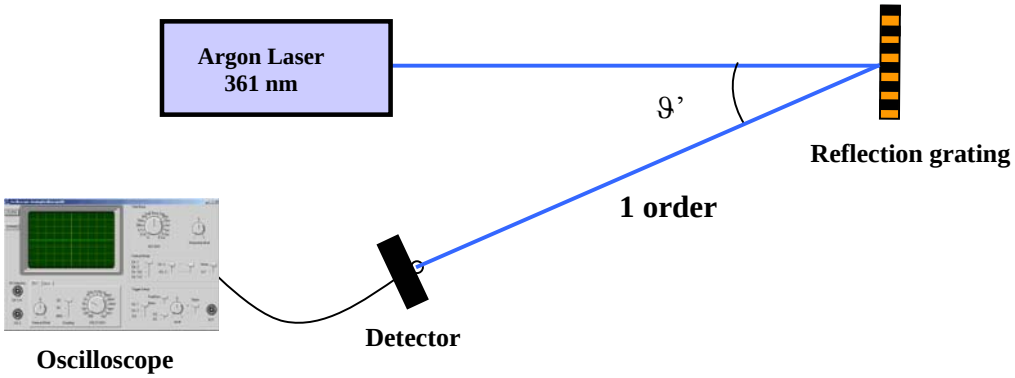

Figure 4.10: Fabry – Perot interferometer system.

The laser beam is partly reflected and partly diffracted by a reflection grating. The diffracted component is analized by a detector. As we can see in the picture above, an angular variation of the diffracted beam, generates also an intensity variation *I(θ)* on the detector because the detector has a pinhole in front with the same dimensions of the impinging beam. By using the grating equation, it is possible to express the relationship between wavelength and diffraction angle:

$$\begin{cases} n\lambda = \Lambda(\sin\vartheta \pm \sin\vartheta') \\ \sin\vartheta = 0 \\ n = 1 \end{cases} \quad \Rightarrow \quad \lambda = \Lambda(\sin\vartheta') \tag{3}$$

where, ϑ (reflection angle) is zero because we are at normal incidence, ϑ' (diffracted angle) is 45°, *n* is equal one because we consider the first diffraction order, λ (361nm) is the wavelength of the used source laser, Λ (400 nm) is the fringe spacing of the grating. By differentiating both members of eq. 3, it is possible to derive the wavelength variation Δλ as:

$$\frac{\Delta\lambda}{\lambda} = \frac{\Delta\Lambda}{\Lambda} + \frac{\Delta(\sin\vartheta')}{\sin\vartheta'} \approx \frac{\Delta(\sin\vartheta')}{\sin\vartheta'}$$

$\Delta\Lambda \approx 0$ because the fringe spacing of the grating is constant. Hence, with a good approximation, the angular variation is proportional to the intensity variation. This means:

$$\frac{\Delta\lambda}{\lambda} \propto \frac{\Delta I(\vartheta')}{I(\vartheta')} \quad \Rightarrow \quad \Delta\lambda \propto \lambda \frac{\Delta I(\vartheta')}{I(\vartheta')} \tag{4}$$

If we measure the intensity variation over time, using the last equation we can determine the wavelength variation. We show the experimental results in figure 4.11:

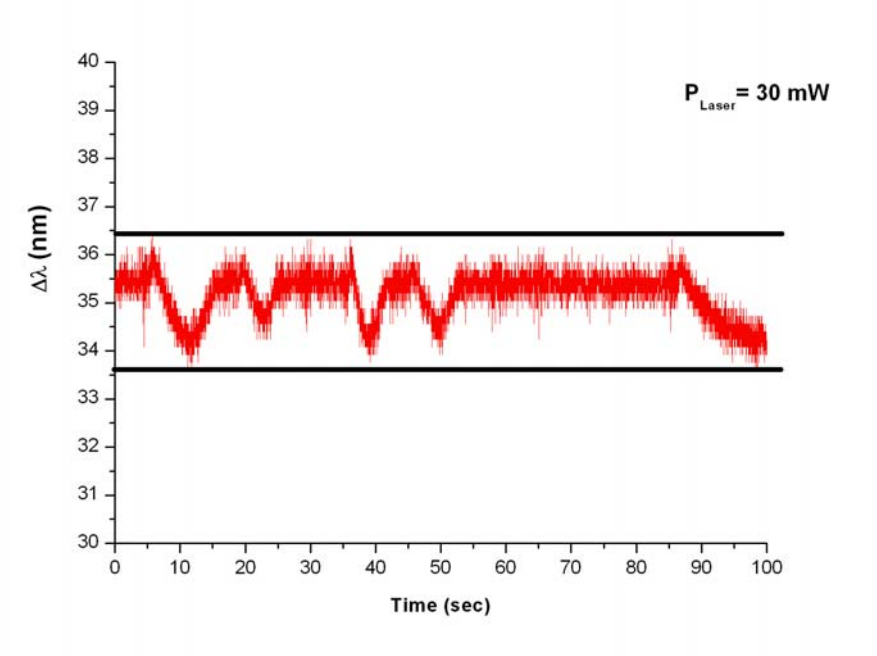

Figure 4.11: Wavelength variation over the time using a laser power of 30 mW.

As shown in figure 4.11, the typical wavelength variation is +/- 3 nm. This means that in this power range this laser source is sufficiently stable for this kind of experiments.

4.5 REALIZATION OF SAMPLES

The fabrication of holographic gratings involves the exposure of a photosensitive material (photo-resist) to an interferometric pattern produced by a laser[38]. In particular we used a positive photo-resist AZ1518 that contains a photoactive compound sensitive to the whole UV-spectrum (310-440) nm. The AZ1518 photo-resist was spin coated onto glass substrates of 2 by 2 cm in size, which were prepared in a clean room to ensure their purity. The cleaning process can be resumed in the following steps:

- Rinse the glass plates with demiwater
- Vibrate (ultra sonic bath) the glass plates for +/- 5 minutes in the "*Teepol*" (soap) solution
- Scrub the glass plates on both sides with a sponge and the *Teepol*-solution.
- Vibrate the glass plates again in the *Teepol* -solution
- Rinse the glass plates careful with demiwater
- Rinse the glass plates for +/- 10 minutes with demiwater in the dip bath.
- Branson(cleaning machine):

  5 minutes ultra sonic vibrating in 60 °C deconex-solution
  10 minutes mega sonic vibrating in 60 °C demiwater
  Rinse +/- 20 minutes with 60 °C clean demiwater
  Dry +/- 20 minutes in hot air dryer

After that, a very thin layer of photo-resist material is deposited on the cleaned substrates by use of a spin coater. The rotation regime of this device and/or the mutual chemical concentration of the photo-resist and a solvent (thinner) can be varied allowing the precise "tuning" of the polymer layer thickness.

We can show in the following graph the dependence of the thickness of the layer versus the thinner concentration for a fixed spinning regime (2000 rpm/30 s)

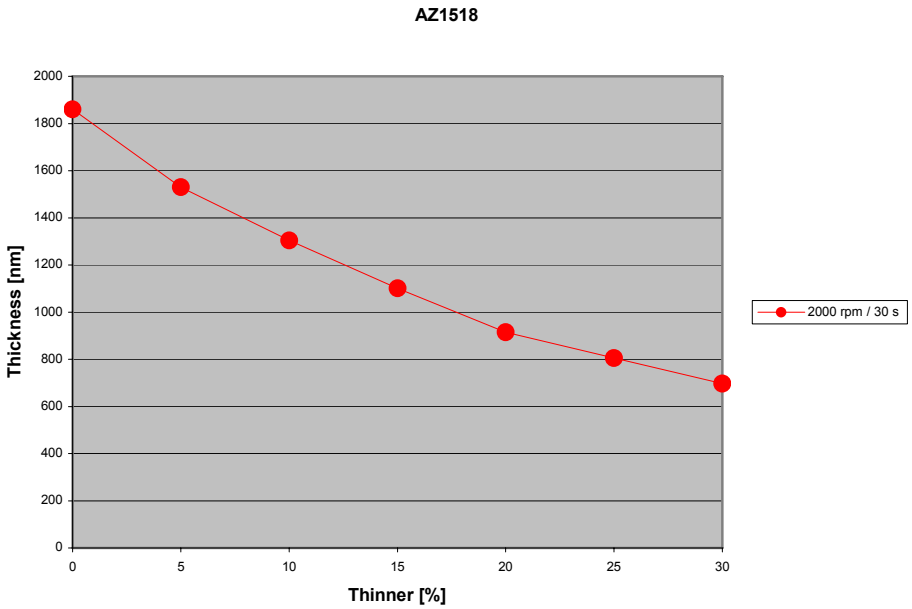

Figure 4.12: Layer thickness over thinner concentration.

The layer thickness can also be varied by changing the spin coater parameters (speed, acceleration and time). In our particular experiment we used a mixture of AZ1518 photo-resist with 10% thinner concentration (5000 rpm/40 s)
The layer thickness has been measured by a standard ellipsometry technique. After spin coating deposition, samples were pre-baked for 10 minute at 90 °C and then exposed to the 361 nm line of an Ar laser by using a holographic set-up (Figure 4.6).

After exposure, a developing procedure is needed to obtain the final structures. The step-by-step recipe for the development is the following:

1. Put 150 ml AZ1518 developer and 150 ml demiwater in a reservoir and mix
2. Develop the sample for 1 minute. (Move the edges of the reservoir by hand, so the mixture will flow from one side to the other).
3. Rinse with demiwater for 1 minute
4. Dry the sample at 60 °C for +/- 15 minutes

The whole process, for preparing grating structures, is represented in the following sketch:

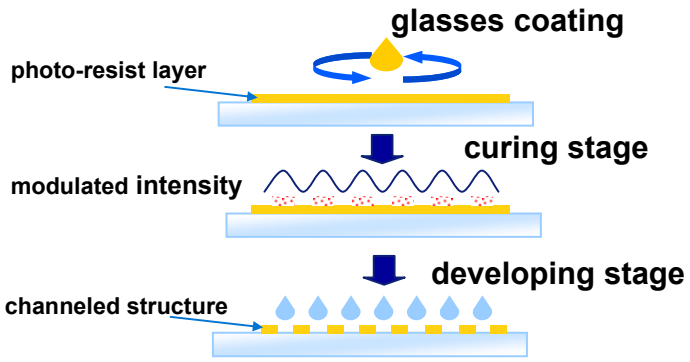

Figure 4.13: Sketch of the whole process for the realization of grating structures

An important parameter in order to realize a periodic structure on a photosensitive material is the light absorbed by the photoresist during exposure, called photoresist dose. It is related to the curing time and curing power, namely:

$$[D]=[P]*[t]=watt*sec=joule$$

P is the curing power and *t* the curing time. By changing these two parameters it is possible to control the depth of the obtained grating. Depending on the dose, it is possible to obtain different morphology for the gratings. As, already introduced above, in the case of a positive photoresist, the light “digs” inside the material. Hence, it can be easily understood that by increasing the dose it will result in deeper structures. It must also be considered that an extremely high dose can completely erase away all the photoresist material resulting in no grating at all. This case can be defined as “over-exposition”. In the opposite case, when the dose is very low the photoresist layer can remain practically untouched. This case is instead called “under-exposition”. It can be easily deducted then that, when dealing with these materials at the beginning, a series of experiments is needed to identify what is the optimal dose range. This empirical “calibration”, also ensures the reproducibility of the experiments. As it can be seen from the dose formula, one particular dose can be obtained by opportunely varying P and t parameters. This can be very helpful when, for example, the laser power is limited because the same dose can be obtained by increasing the exposure time.

4.6 GRATING STRUCTURES REALIZATION

The used holographic interferometer is similar to the one shown in figure 4.6. Prior to being split into two separate beam paths, the laser beam is scanned with a very small pinhole, of about 500 μm, mounted on a photodetector. Using a translation stage it is possible to shift the detector in the direction transverse to the incident beam. An intensity profile can be obtained, in such away that we show in the following picture:

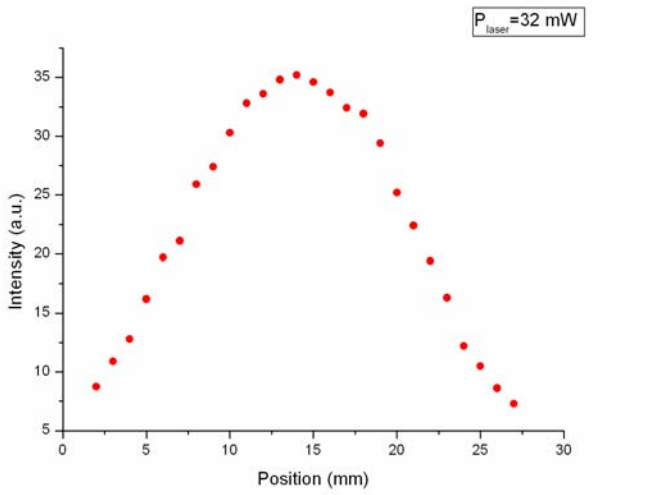

Figure 4.14: Beam profile of the laser in our setup at a power of 32 mW.

The resulting profile resembles a Gaussian shape. As shown in the first chapter section (figure 1.3), in order to work with a periodic and regular interference pattern it is convenient that the used profile is flat.

One simple reason is that if the intensity is not uniform the curing dose will not be constant. This produces regions with different exposures on the spot of the curing grating and it is possible to obtain over-exposed and under-exposed areas.

With a small aperture (of about 1 cm) it is possible to select the central part, of the total intensity profile and with a good approximation we can work with a flat profile.

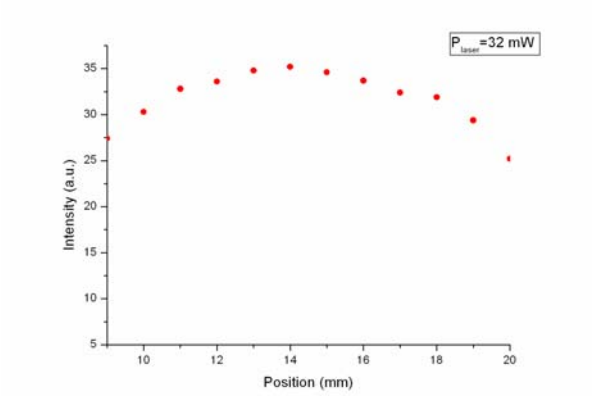

Figure 4.15: Flat profile obtained using the central part of the original beam

In order to check the reliability of our experimental setup, we proceeded with a series of experiments with several fringe spacing. For every fringe spacing we checked the morphology and tried to correct possible mistakes. We started with a big fringe spacing in order to check the quality of the obtained gratings with simple means like an optical microscope. After that, if the morphology looked nice, we could decrease the fringe spacing and try to estimate whether the stability degree of the used set-up is enough for our experiments. The first experiments were realized with 10 μm of periodicity that corresponds to an incidence angle of 1.1deg. For these preliminary experiments we have empirically found the best curing parameters reported in the following table:

Plaser (mW)	**Curing voltage** (mV)	**Curing time** (sec)
33	**320**	**120**

These parameters have been chosen just by judging the grating morphology. No other optical properties have been considered at this preliminary stage.

The values have been measured by using a broad range photo-detector in order to know a reference value for a single curing beam. Using this value the obtained sample is generally uniform and there are no over and under exposed regions. The morphology of the grating by analysis with a standard optical microscope is like in Fig. 4.16.

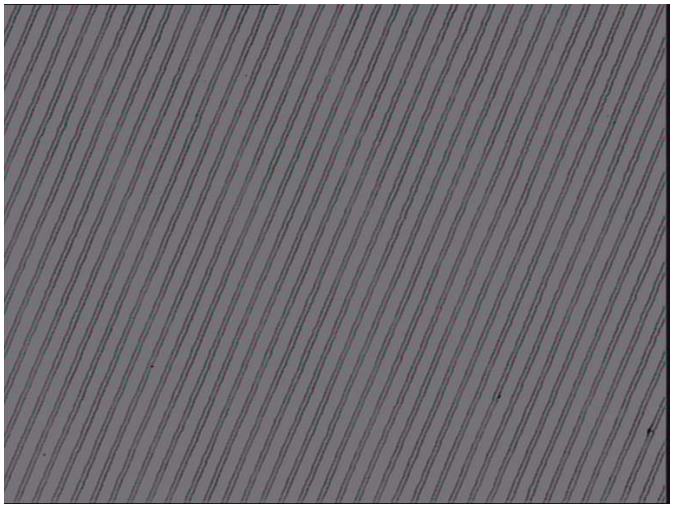

Figure 4.16: Grating morphology obtained by using an optical microscope (Λ= 10 μm)

As already said, the obtained grating present a constant periodicity, by checking different areas it looks also uniform. After that, we reduced the fringe spacing to 2µm. The best curing parameters obtained, after several experiments, are in this case:

Plaser (mW)	**Curing voltage** (mV)	**Curing time** (sec)
28	**431**	**26**

In order to check this morphology we used a different optical microscope, because we needed a bigger magnification.

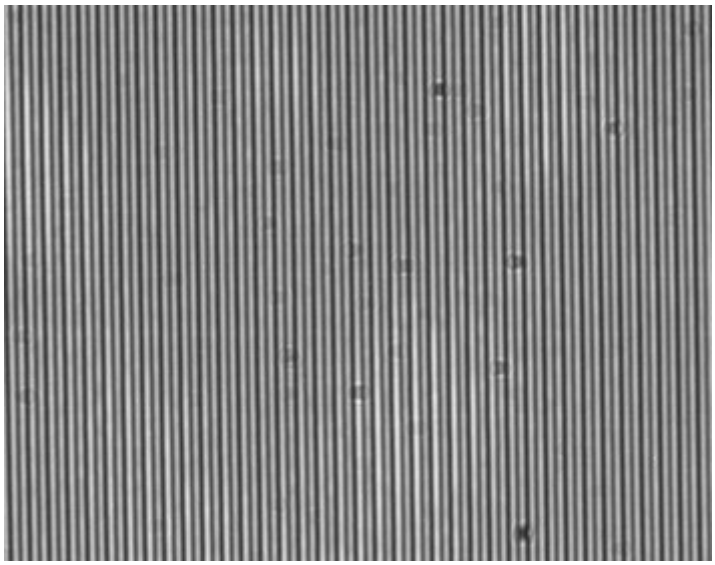

Figure 4.17: Grating morphology obtained by using an optical microscope (Λ= 2 μm)

In the next paragraph we will relate this morphology to the optical properties of the grating.

4.7 OPTICAL CHARACTERIZATION

One of the most useful optical parameter to measure the quality of a diffraction grating is the diffraction efficiency (DE). We define diffraction efficiency as the ratio of the intensity of the desired diffracted beam and the intensity of the incidence beam. Diffraction efficiency $DE = f(\theta_{inc}, \lambda, d, \Delta n)^2$ is a function of the incidence angle, wavelength, grating depth, index modulation. By optimizing these parameters it is possible to obtain grating structures with high value of diffraction efficiency. Our setup for measuring the diffraction efficiency is shown in fig. 4.18:

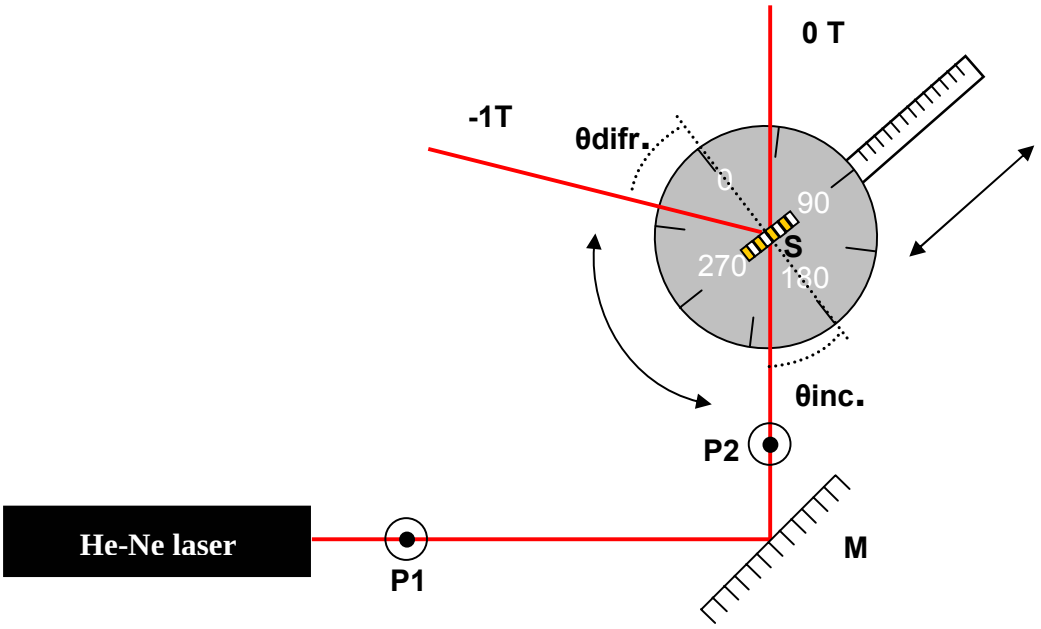

Figure 4.18: Optical probing setup for characterization gratings; **M,** mirror; **P1, P2,** polarisers; **S,** sample; **0T,** zero order transmission; **-1T,** first order transmission; **θinc,** incidence angle; **θdifr,** diffracted angle.

A polarized He-Ne laser beam (λ= 633 nm) is directed on the sample with an incidence angle θ_{inc}. The beam is transmitted and diffracted by the grating.

The sample is mounted on a holder with both a translation and a rotation stage. In order to check whether the morphology of the grating showed in figure 4.17 (Λ= 2 μm) is uniform or not, we fixed the probe incidence angle and measured the diffraction efficiency by shifting the grating in a direction perpendicular to the fringes of the grating, in such away it is possible to check different points of the grating area.

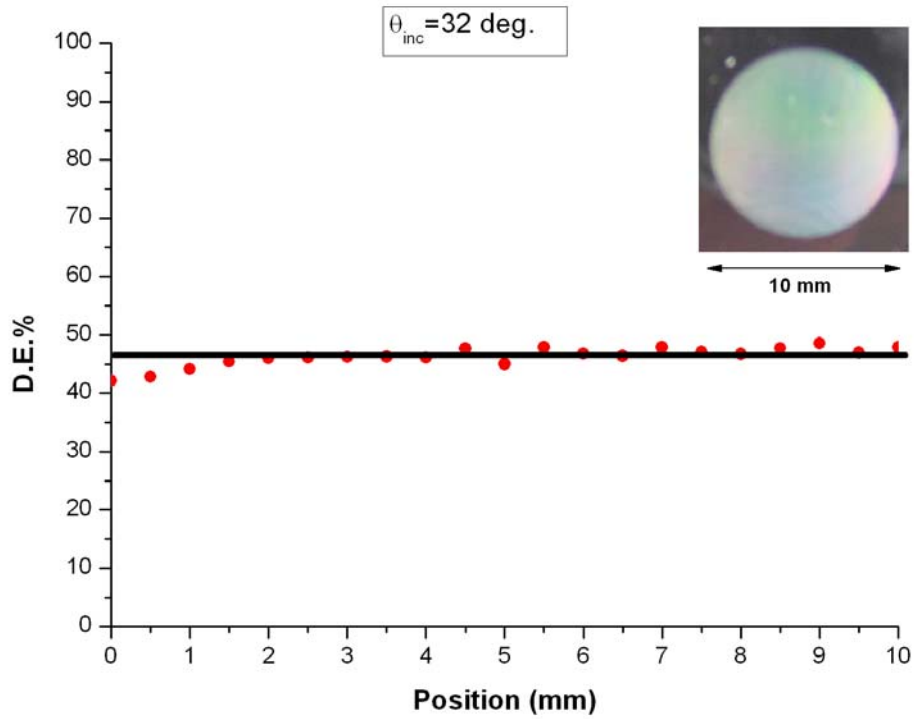

Figure 4.19: Diffraction efficiency as a function of the position of the grating

As we can see, in the picture above, the diffraction efficiency is reasonably uniform. There are some variations on the border of the grating, probably due to the not perfectly flat intensity profile (see Fig.4.15).

4.8 OPTMISING GRATING STRUCTURES FOR COLOUR-SEPARATING BACKLIGHT

As already said, the diffraction efficiency depends of different parameters. In order to optimize these parameters a commercially available computer program GSOLVER[39], based on the rigorous coupled-wave theory[2], was used to determine the best grating parameters. By fixing the fringe spacing (Λ=400 nm, because for our application of colour separation we want the green along the normal) we performed simulations to find the optimum grating depth in order to maximize the diffraction efficiency[40]. .

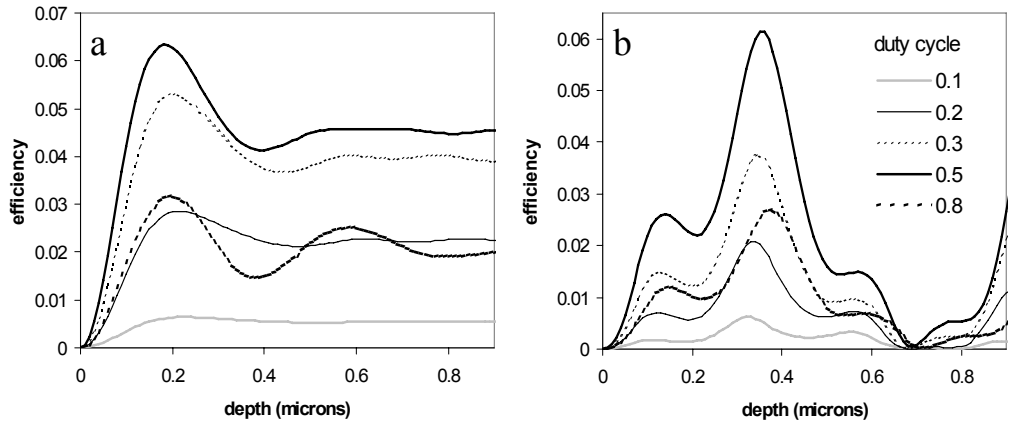

Figurte 4.20. Calculated diffraction efficiency versus the grating depth by fixing the incidence angle and the probing wavelength for various duty cycles. a) Grooves filled with low-index material (n = 1), b) grooves filled with high-index material (n = 1.77).

In Figure 4.20a the diffraction efficiency is plotted as a function of the depth of the grating for various values of the duty cycle (i.e. the ratio between the widths of polycarbonate and air). The reason for the oscillating behaviour is that, with the depth having an order of magnitude of the wavelength, the grating acts as an interference layer. It is found that a duty cycle of 0.5 is optimal, whereas the optimal depth is around 200 nm.

In Fig. 4.20b we show simulations for the case that the grooves are filled with a material of high refractive index (1.77, equal to the n_e of the liquid crystal that we will use below).

The oscillations due to interference are now even more pronounced, with a minimum at 700 nm. The optimal depth for this case is around 400 nm. By choosing 400 nm as fringe spacing of the grating it is possible to see, using the *thin e thick theory*[1] introduced by Gaylord et al., that also the Bragg diffraction regime is obtained. By considering this theory it comes out that an important parameter is the ratio between the grating depth (d) and the fringe spacing (Λ). $\Lambda/d<10$ a grating can be considered in Bragg diffraction regime, namely, only one diffraction order is present. Making a simple calculation we can verify that for a fringe spacing of 400 nm we are in Bragg regime. In order to obtain good gratings with this periodicity. the best curing parameters are:

Plaser (mW)	**Curing voltage** (mV)	**Curing time** (sec)
30	**450**	**23**

In this case, we were obliged to use scanning electron microscopy (SEM in order to analyze the morphology of the obtained grating.

We show in the following picture the obtained result:

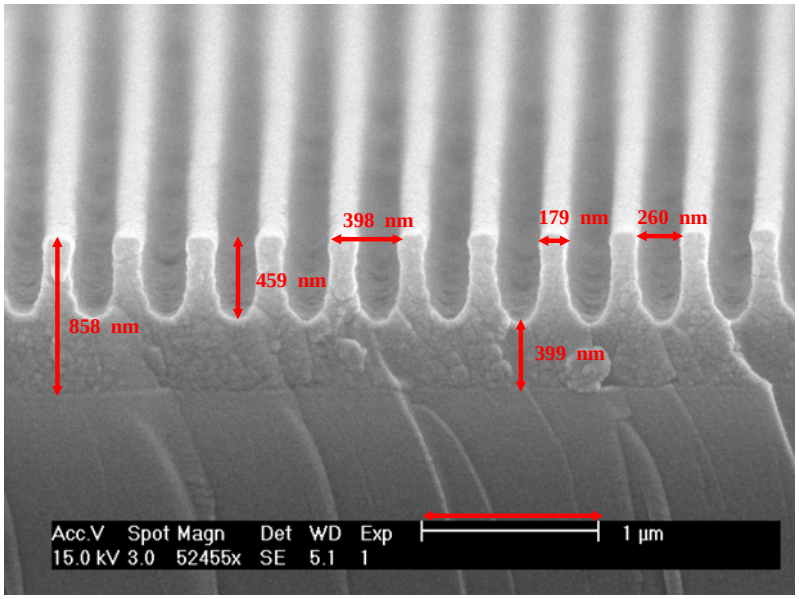

Figure 4.21: SEM pictures of grating structure, grating in AZ1518 with depth approximately 459 nm, fringe spacing 398 nm, resist layer 858 nm, resist channels 179 nm, air channels 360 nm, uniform layer under the grating 399 nm..

As we can see the morphology looks nice and regular. It is worthwhile to consider that we start with a sinusoidal profile of the interference pattern but the grating profile we get is square. This is due to the nonlinear response of the photo-resist material, to the curing intensity. Namely, the photoactive material does not react at all until a given intensity threshold is not reached. Also in this case, in order to check the uniform diffraction efficiency we used the same setup shown in fig. 4.18 and the same trick of measuring DE with a given angle and shifting over the grating surface.

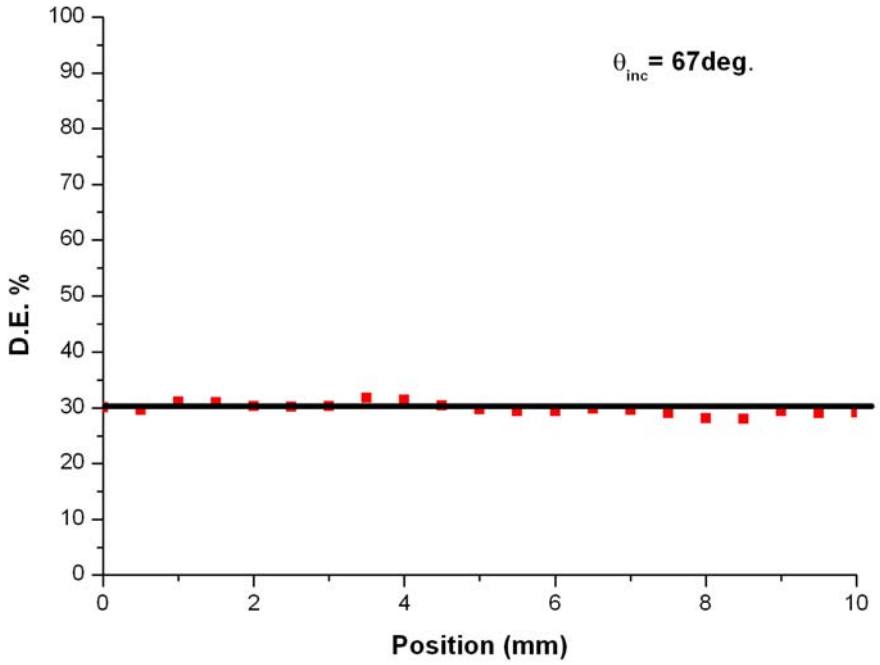

Figure 4.22: Diffraction efficiency over the position of the grating

As we can see the diffraction efficiency is sufficiently uniform, this implies that the grating depth is approximately constant all over the spot. Different grating depths can be obtained by varying the dose (curing power or curing time).

4.9 LARGE AREA GRATING OBTAINED WITH A STEP AND REPEAT PROCESS

The possibility of using the obtained gratings for display applications require a typical grating area comparable with a standard monitor size. We are able to realize very uniform gratings but their typical sizes (1 cm) are not suitable for our application. As a possible way to solve this problem has been found an original solution. In detail, by using a square mask it is possible to realize an interference pattern with the same shape. The idea is to shift in both x and y directions a big sample in front of this UV square pattern in a step-and-repeat process in order to obtain a precise “patterning” constituted by contiguous square gratings. In principle this patterning could cover very large areas.

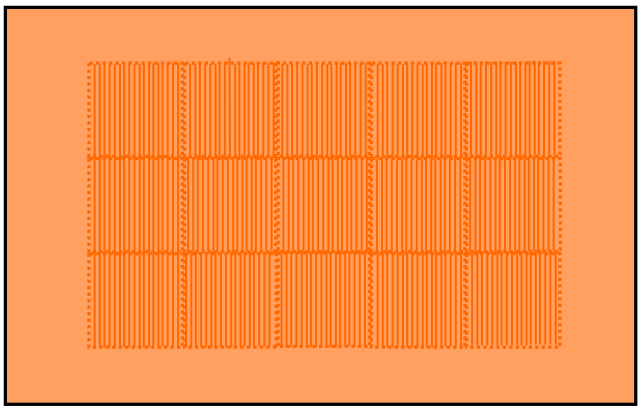

Figure 4.23: Large area grating obtained by using a step and repeat process

The setup used in order to realize a big grating by combining multiple exposure is approximately the same as shown in Figure 4.6, the main differences are:

1) A square aperture put after the lens L2, in order to cut a square profile.
2) A two-dimensional translation stage where the sample S has been mounted.

The bidimensional translation stage allows to shift the glass plate after each curing process. We show in the following picture the utilized mechanical system:

Figure 4.24: Two-dimensional translation stage with sample holder.

An important role is played by the perfect alignment of the curing beams. If some misalignment is present, like for example the not perfect overlapping of the two curing beam in both direction, a uniform curing will be present on the upper or left borders. Namely, on the borders is present a uniform intensity which completely removes the photo-resist regions between two adjacent gratings

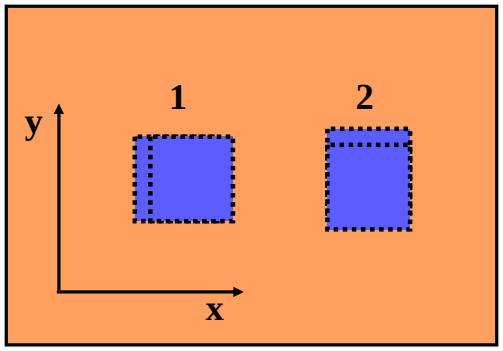

Figure 4.25: Possible misalignment condition in both direction (**1**, long x; **2** long y) due to the non perfect overlapping of the curing beams.

If any of these conditions is present, or both of them, the final result will look like a checkerboard. Namely, different gratings with a small area between them where there is no grating. In order to avoid this problem, a very precise check on the alignment has been performed before exposing the sample. We can show the measurement as a function of the diffraction efficiency over position on a grating of 24 mm realized in four steps.

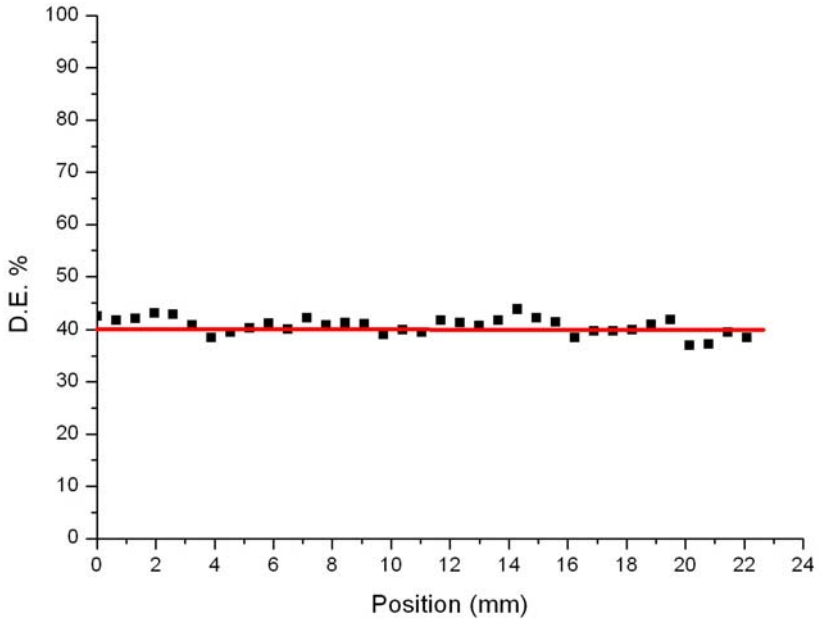

Figure 4.26: Diffraction efficiency as a function of the position of the grating..

Also in this case the diffraction efficiency looks uniform, even if some small variations are present. Probably they are due to the presence of the Fresnel diffraction pattern and to the not perfect splice between two adjacent gratings. Using a square mask, to cut the central part of the circular initial beam, a Fresnel diffraction will result on the pattern.

Using a commercial and free applet[41], it is possible to simulate the situation in which a wave plane incomes on a square slit. We have chosen a square aperture of 6 mm and a distance, between the aperture and the screen, of 30 cm.

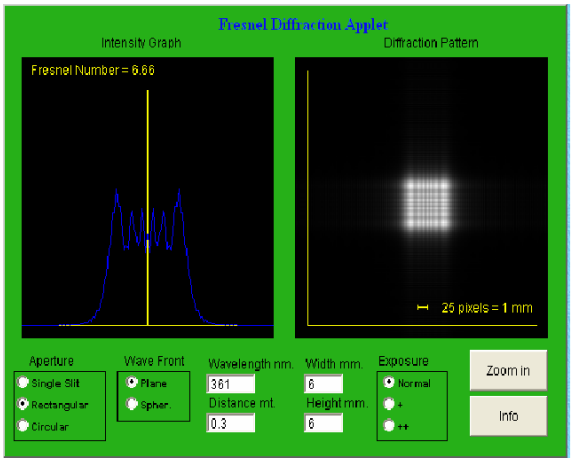

Figure 4.27: Diffraction of light through a bidimensional aperture according with Fresnel theory. The left windows shown the intensity distribution and the Fresnel number. The right window shows the diffraction pattern.

As we can see on the right part of the figure, a periodic square pattern is present with a visible periodicity. This means also that this modulation will be not a problem for our experiment because its typical size is not comparable with the grating periodicity. Another improvement could be realized with a translation –motor-driven nano-positioning system in order to increase precision and speed of the total process.

4.10 COLOUR-SEPARATING BACKLIGHT: EXPERIMENTS

For our experiments we used a glass substrate lightguide (refractive index n = 1.5) with a grating in AZ1518 (n=1.59) applied on it, having a period of 398 nm and a modulation depth of 459 nm (checked with SEM) made via laser-interference lithography. This structure was placed in a side-lit configuration with a cold-cathode fluorescence lamp (CCFL). We characterised the angular distribution of the outcoupled light for the three basic colours with a DMS-803 from autronic-Melchers[42] (Figure 4.27).

Figure 4.28: AUTRONIC-MELCHERS, DMS-803 series.

To measure electro-optical performance of liquid crystal displays autronic-Melchers provides the DMS (*Display Measuring System*) series. These systems combine synchronized driving and data acquisition / sampling with a high precision positioning mechanism, thus, providing the capabilities to measure electro-optical characteristics, response time and contrast distribution. With AUTRONIC system it is possible to realize an angular scan in the range 300-800 nm.

The Spectro-radiometric detector of the DMS is a Multi-channel Spectro-radiometer, connected to the measuring microscope via a quartz light fiber bundle. It comprises the following main components:

- Entrance optics
- Electro-magnetical shutter for measuring the dark counts (“background”)
- Entrance slit
- Holographic grating as dispersing element
- CCD image sensor (1024x128 elements)

We show a spectral analysis of the used light source:

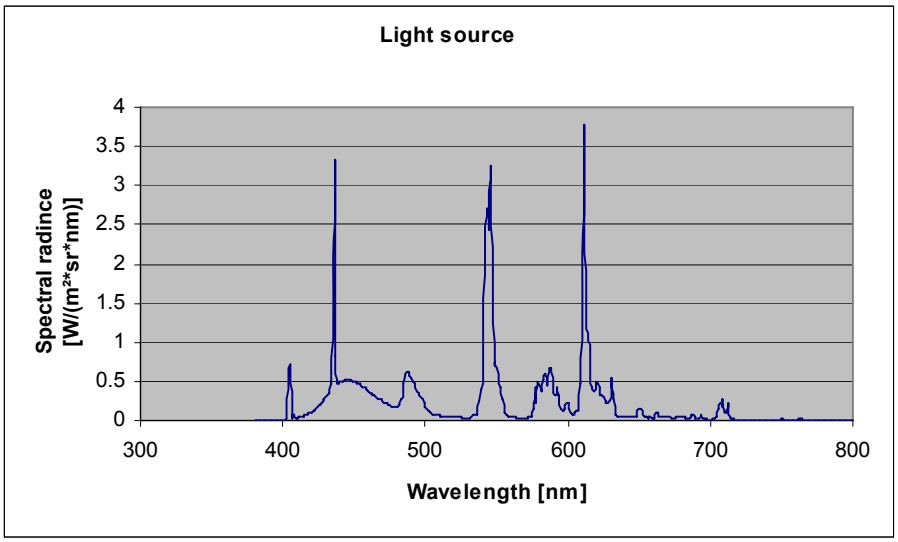

Figure 4.29: Spectrum of the light source.

This measurement has been realized positioning the detector direct in front of the source. We can see the characteristic CCFL spectrum due to the standard red, green and blue phosphors.

In order to check the influences of the resist (AZ1518) on the light source, we used a glass substrate covered with a resist layer. The light was diffused out through the resist layer by a piece of scattering tape. The diffused light has been monitored in the same way as the previous experiment. We can show the obtained results:

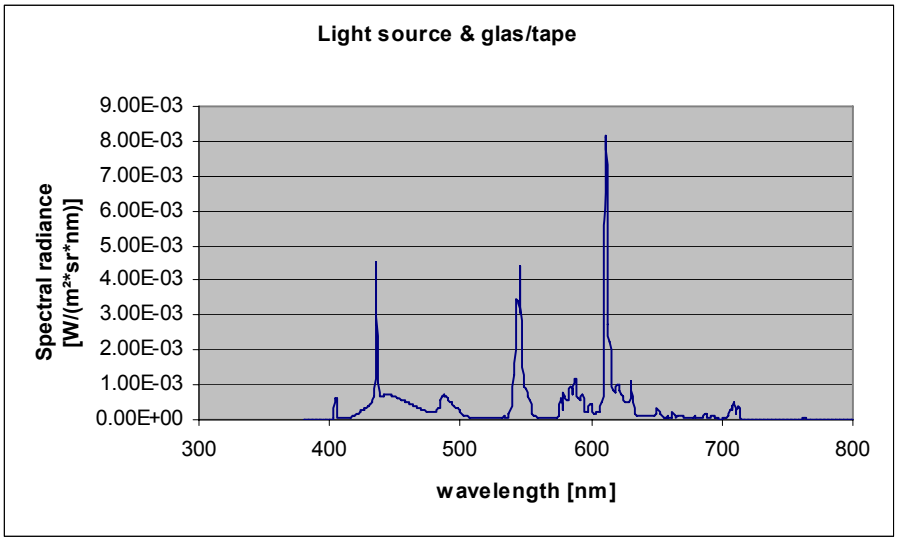

Figure 4.30: Light source with glass tape spectrum analysis

As shown, in the range 400-600 nm, the material is not completely transparent. The green and blue lines present a smaller luminosity with respect to the red line. This means also that the device will not be efficient in this range. Anyway this resist material was chosen for simple, pratical experimental reasons. Making gratings with this material is relatively easy. In order to improve the efficiency in future we will try to replicate these structures in other materials. A replica process can be realized using a uniform structure obtained with this material as a master. Afterwards it is possible to realize a copy in a different material which present different properties useful for our application.

We studied an illumination system using a total internal reflection lightguide and a diffraction grating. We found that if the emitted light from a white light source such as a tri-band fluorescent lamp enters a grating sheet having a pitch of 400 nm, the diffracted output light has three primary colour components with different exit angles depending on the wavelength, and three colours are directionally separated according to the grating equation:

$$\sin\theta_{out} = n\sin\theta_{in} + m\lambda / \Lambda$$

where Λ, λ, θ_{in}, θ_{out}, n, and m, denote the grating pitch, the wavelength, the incident angle, the exit angle, diffraction index, and an integer specifying the diffraction order. In the following picture we can show a tipycal immagine of a colour separating backlight

Figure 4.31: Colour separating backlight

We send a light, inside a light guide with on top a grating. The grating grooves are ortogonal to the propagation direction of the incident light. On a white screen it is possible to see the three main colours of the used light source. In the angular distribution, curved regions are seen with blue on top, green in the

centre and red at the bottom. Using the spectroradiometer CCD of the Autronic system it is possible to check the angular distribution along the θ direction.

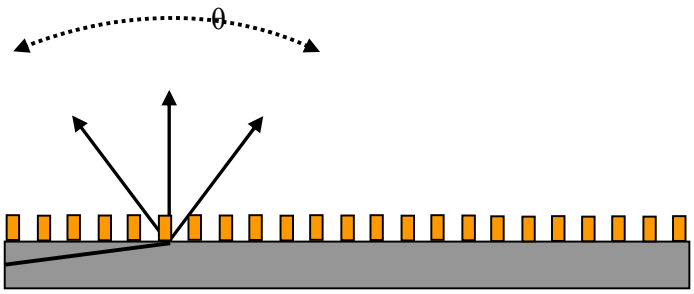

Figure 4.32: Schematic AUTRONIC measurement.

The CCD detector has been focused, with a lens system, on an area of the grating of 0.5 mm. The “camera” was mounted on a mobile arm controlled by a standard pc. It has been possible to scan the outcoupled intensity in the θ direction in the range +/-70˚. The obtained results are:

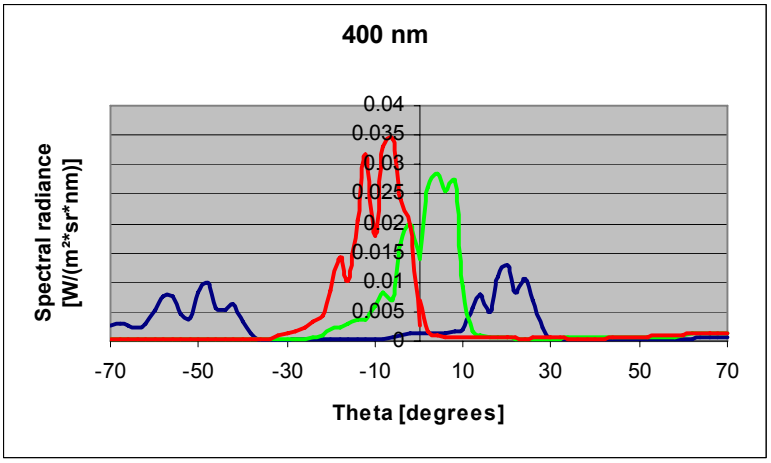

Figure 4.33: Measurement angular distribution

We obtained that the three main CCFL lines due to red, green and blue phosphors are coupled out in slightly overlapping angular regions between -30^{o} and $+30^{o}$. There is also some blue light in the -2^{nd} order at large negative angles. The graph of Fig.4.33 shows the measured intensities for the main phosphor lines (at 610, 535 and 435 nm) in the direction perpendicular to the grooves. As we can see, in the three curves some intensity oscillation is present. Probably this is due to the angular distribution of the light inside the light guide, namely, they are due to the deviation from a perfect Lambertian distribution of the light at the entrance of the light guide. This, will produce the observed oscillation at the outcoupled intensity.

CONCLUSIONS

Diffractive colour separation is an innovative technique useful to obtain an efficient LCD system. By using a periodic structure on top of a light guide colour separation can be realize. In this work the attention has been focalized on the realization of such a periodic structure using holographic means.

The realization and characterization of an holographic diffraction grating has been carefully considered. The starting point has been the realization of an holographic setup and characterization of its stability. By using a stable and homogenous interference pattern it has been possible to realize a periodic structure with good optical properties on a photosensitive material. A key check parameter for an holographic diffraction grating is the diffraction efficiency. The realized structures present good and uniform diffraction efficiency. In order to realize large area grating a nice and innovative technique has been invented, we proposed to call it "*Step and repeat process*". By using a square interference pattern has been possible to stick on the same glass substrate different gratings. An improvement could be obtained with a translation –motor-driven nano-positioning system in order to increase precision and speed of the total process. In principle, this is a cheaper and simple way in order to realize large area gratings. The colour separation backlight is the heart of this work. By using an autronic-Melchers has been possible to realize an angular scan of the outcoupled intensity. The three main CCFL lines due to red, green and blue phosphors are coupled out in slightly overlapping angular regions between -30^{o} and $+30^{o}$. For the future, different improvements can be realized by changing the geometry of the system or by using different materials.